AIAA JOURNAL
Vol. 38, No. 5, May 2000

Aeroelastic Analysis of a Hingeless Rotor Blade in Forward Flight

Seong Min Jeon* and In Lee†
Korea Advanced Institute of Science and Technology, Taejon 305-701, Republic of Korea

The aeroelastic response and stability of isotropic and composite rotor blades are investigated using a large deflection-type beam theory. The finite element equations of motion for beams undergoing arbitrary large displacements and rotations, but small strains, are obtained from Hamilton's principle. The sectional elastic constants of a composite box beam including warping deformations are determined from the refined cross-sectional finite element method. The analysis is performed for a soft-in-plane hingeless rotor in free flight propulsive trim. The nonlinear periodic blade steady response is obtained by integrating the full finite element equation in time through a coupled trim procedure with a vehicle trim. After the coupled trim response is computed, the aeroelastic response is calculated through a time-marching solution procedure under small perturbations assumption, and then the stability analysis is performed by using a moving block analysis. Numerical results of rotating natural frequencies, blade response, and aeroelastic stability are presented. The results of the full finite element analysis using the large deflection-type beam theory are quite different from those of a previously published modal analysis using the moderate deflection-type beam theory.

Nomenclature

$\boldsymbol{A}, \boldsymbol{B}, \boldsymbol{D}$	= effective sectional stiffness matrix
C_T	= thrust coefficient $[T/\rho_a \pi R^2 (\Omega R)^2]$
c_d	= profile drag coefficient
c_l	= lift coefficient
$\boldsymbol{e}_1, \boldsymbol{e}_2, \boldsymbol{e}_3$	= reference orthogonal unit vectors in the undeformed configuration
$\boldsymbol{e}_1^*, \boldsymbol{e}_2^*, \boldsymbol{e}_3^*$	= reference orthogonal unit vectors in the deformed configuration
$\bar{e}_{11}, \bar{e}_{12}, \bar{e}_{13}$	= strain vectors at reference point
$\boldsymbol{I}_1, \boldsymbol{I}_2, \boldsymbol{I}_3$	= inertia frame fixed orthogonal unit vectors
$\boldsymbol{i}_1, \boldsymbol{i}_2, \boldsymbol{i}_3$	= rotating hub fixed orthogonal unit vectors
k_A	= polar radius of gyration of blade cross section
k_{m1}, k_{m2}	= principal mass radii of gyration of blade cross section
$\boldsymbol{q}$	= generalized nodal displacement vector
R	= blade radius
$\boldsymbol{T}(x_1)$	= transformation matrix between deformed blade axis and rotating hub axis
$\boldsymbol{t}_e(x_1)$	= transformation matrix between undeformed blade axis and deformed blade axis
$\boldsymbol{t}_g(x_1)$	= transformation matrix between undeformed blade axis and rotating hub axis
U_R, U_T, U_P	= radial, tangential, and perpendicular components of blade section resultant velocity U, respectively
u_1, u_2, u_3	= components of displacement vector $\boldsymbol{u}$
v_{id}	= induced inflow velocity
x_1, x_2, x_3	= blade curvilinear coordinates
W_1, W_2, W_3	= warping displacements
$\kappa_1, \kappa_2, \kappa_3$	= difference between undeformed and deformed strain curvature vectors
λ_i	= induced inflow ratio
μ	= advance ratio
σ	= blade solidity $(N_b c/\pi R)$
ψ	= azimuth angle, Ωt
Ω	= rotor blade angular velocity
$(\,)_{,i}$	= $\partial(\,)/\partial x_i$, $i = 2, 3$
$(\,)'$	= $\partial(\,)/\partial x_1$
$(\dot{})$	= $\partial(\,)/\Omega\partial t = \partial(\,)/\partial\psi$

Received 13 May 1999; revision received 16 September 1999; accepted for publication 16 September 1999.

*Graduate Research Assistant, Department of Aerospace Engineering, 373-1 Kusong-dong, Yusong-gu.

†Professor, Department of Aerospace Engineering, 373-1 Kusong-dong, Yusong-gu. Senior Member AIAA.

Introduction

ENHANCED research on aeroelastic analysis of hingeless rotor blades has been performed to understand physical phenomena during the past decade.[1] Aeroelastic analysis is inherently a nonlinear phenomenon because the hingeless rotor blade has a geometrical nonlinearity caused by structural characteristics. Also, recently developed composite rotor blades induce a complex task such as existence of coupling stiffness, transverse shear, and warping.[2] The geometrical nonlinearities caused by blade deflections play an important role in the aeroelastic characteristics of the hingeless rotor blade,[1] and the nonclassical structural effects of a laminated structure have a considerable influence on the static and dynamic behavior compared to that of a homogeneous isotropic structure because of a very low transverse shear modulus of composites compared to inplane tensile moduli.[3]

Up to now, research on composite rotor blades has been performed for global deformation and cross-sectional analyses in a wide scope. One-dimensional global deformation analyses of rotor blades considering the geometrical nonlinearity have been classified into two-type beam theories of a moderate deflection-type and a large deflection-type. Since Hodges and Dowell[4] developed a moderate deflection-type beam theory, it has been developed to investigate static[5–7] and dynamic[8–10] behavior of composite beams. However, these models impose artificial restrictions on displacements and rotations caused by the deformation and the degree of nonlinearity. To overcome these limitations of previous models, structural models that are valid for large deflections including all kinematic nonlinear effects have been developed for a general purpose during the last few years and used for static[11–17] and dynamic[18–20] analyses of composite beams. It is also important to obtain accurate effective sectional stiffness through the cross-sectional analysis with one-dimensional global deformation analysis. The presence of nonclassical structural effects such as transverse shear and warping have a powerful influence on the behavior of composite beams. The cross-sectional analysis has been carried out using both direct analytical methods[3, 5–7, 14, 21] and finite element methods.[11–13, 16, 22–24] Finite element methods give more accurate results than the analytical methods because it is difficult to obtain exact sectional stiffness of composite beams.

Only a little work has been done to investigate the aeroelastic characteristics of composite rotor blades. Structural coupling of composite blades has a potential for increment of stability and

reduction in vibration levels in hover through aeroelastic analyses based on the moderate deflection-type beam theory.[25,26] This type of beam theory is also extensively applied to examine the dynamics of composite rotors in forward flight,[27,28] and Smith and Chopra[29] improved a method using an advanced structural model and fully coupled trim solution. There are a few studies on the aeroelastic analysis of rotor blades using large deflection-type beam theories compared with previous works, and these type beam theories are applied to isotropic rotor blades[30–32] and composite rotor blades[33–35] only in hover condition. Aeroelastic stability boundaries and steady tip deflections based on these theories are reported to be quite different from those based on the moderate deflection-type beam theories when the collective pitch angle becomes large.[30]

In the present study the finite element approach using the large deflection-type beam theory is presented for the aeroelastic analysis of isotropic and composite hingeless rotor blades in forward flight. The composite rotor blade is idealized as a laminated thin-walled box beam, and effective 6×6 elastic constants are obtained through the refined cross-sectional finite element analysis. The structural model used in the present analysis is modified from Bauchau and Hong's beam model,[12] and this model is verified through static and dynamic analyses of composite box beams.[20] Nonlinear, periodic blade steady responses are obtained using Borri's time finite element method[36] on a full finite element equation in forward flight condition. Blade responses fully coupled with vehicle trim should be solved to obtain nonlinear blade response, pilot controls (collective and cyclic pitch of a main rotor and collective pitch of a tail rotor), and vehicle attitude (longitudinal and lateral shaft tilt angles). Assuming blade motions to be small perturbations about nonlinear periodic equilibrium positions, the aeroelastic response is determined through a time-marching solution procedure, and then the stability analysis is performed using a moving block analysis. The full finite element results using the large deflection-type beam theory are compared with the results obtained by modal approach using the moderate deflection-type beam theory.

Analysis

Kinematics

Consider the rotor blade rotating with angular velocity Ω depicted in Fig. 1. Here the triad $\boldsymbol{I}_1$, $\boldsymbol{I}_2$, and $\boldsymbol{I}_3$ is fixed in an inertia frame; the triad $\boldsymbol{i}_1$, $\boldsymbol{i}_2$, and $\boldsymbol{i}_3$ fixed in a reference frame, which rotates with respect to the inertia frame at a constant angular velocity $\Omega \boldsymbol{I}_3$; the triad $\boldsymbol{e}_1$, $\boldsymbol{e}_2$, and $\boldsymbol{e}_3$ attached to a reference line along the axis of the undeformed blade; and the triad $\boldsymbol{e}_1^*$, $\boldsymbol{e}_2^*$, and $\boldsymbol{e}_3^*$ attached to a reference line along the axis of the deformed blade. The geometrical nonlinearities are described using coordinate transformation matrices with the Euler angles in the present large deflection-type beam theory:

$$\boldsymbol{e}_i^* = \boldsymbol{t}_e(x_1)\boldsymbol{e}_i = \boldsymbol{T}(x_1)\boldsymbol{i}_i, \qquad \boldsymbol{T}(x_1) = \boldsymbol{t}_e(x_1)\boldsymbol{t}_g(x_1) \tag{1}$$

The transformation matrices $\boldsymbol{t}_g$, $\boldsymbol{t}_e$, and $\boldsymbol{T}$ are functions of the curvilinear axial coordinate x_1. Assuming that initial curvatures are small and shearing strains are much smaller than unity in the Green–Lagrangian strain components, strain-displacement relations are represented as those in Ref. 12. If we neglect higher-order strain components and initial curvatures and introduce general warping displacements in and out of plane of a cross section, strain-displacement relations can be expressed as follows[20]:

$$\begin{aligned} \varepsilon_{11} &= \bar{e}_{11} + x_3\kappa_2 - x_2\kappa_3 + w_1' \\ \gamma_{12} &= 2\bar{e}_{13} + x_3\kappa_1 + w_2' + w_{1,2} \\ \gamma_{13} &= 2\bar{e}_{13} + x_2\kappa_1 + w_3' + w_{1,3} \end{aligned}$$

$$\varepsilon_{22} = w_{2,2}, \qquad \gamma_{23} = w_{2,3} + w_{3,2}, \qquad \varepsilon_{33} = w_{3,3} \tag{2}$$

where w_1, w_2, and w_3 are the general warping displacements of an arbitrary point on the cross section. The force strains ($\bar{e}_{11}$, $2\bar{e}_{12}$, $2\bar{e}_{13}$) and moment strains (κ_1, κ_2, κ_3) components are given in Ref. 20. Through a quasilinear approximation[16] this three-dimensional kinematics is divided into two-dimensional cross-sectional analysis and one-dimensional global analysis.

Cross-Sectional Analysis

Although the cross-sectional analysis is coupled with the global analysis, effective sectional elastic constants including effects of general warping deformations in and out of plane are easily obtained from a linearization of governing equations with respect to reference state (undeformed and unstressed state). Solutions from these quasilinear equations should be reasonable approximations to obtain the sectional elastic constants used in nonlinear elastic deformation of slender, closed-section composite beams.[16] Cross-sectional analysis of composite beams based on Ref. 22 is performed using the finite element method considering three-dimensional stress and de Saint Venant hypotheses. In the present work the cross-sectional modeling for the box beam is proposed as shown in Fig. 1. The displacement in the thickness direction is interpolated as a linear function and integrated analytically. In the other direction a cubic Lagrangian function is used and integrated using Gauss–Legendre quadrature. The two-dimensional shape function of warping in an element is

$$w(x_1, x_2, x_3) = \sum_{i=1}^{2}\sum_{j=1}^{4} N_i^L N_j^C W_{ij}(x_1) \tag{3}$$

where N_i^L is the linear shape function in the thickness direction, N_j^C the cubic shape function in the width direction, and W_{ij} the warping amplitude. This approach is simpler and more efficient than that

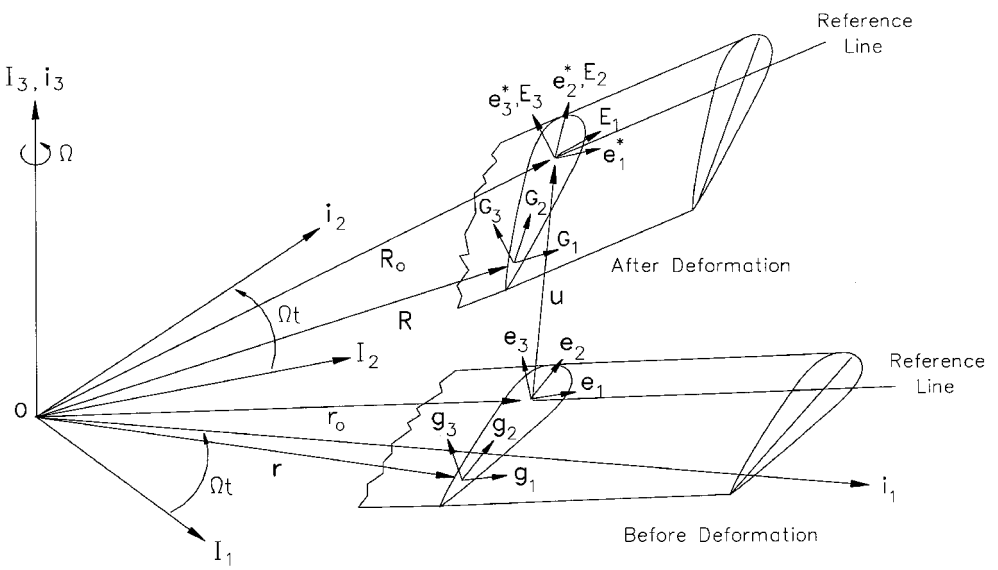

Fig. 1 Geometry and coordinate systems of a rotor blade before and after deformation.

given in Ref. 22 to consider the change of material properties in the thickness direction. In unloaded condition effective elastic sectional stiffness matrix can be obtained as follows:

$$\begin{Bmatrix} \boldsymbol{F} \\ \boldsymbol{M} \end{Bmatrix} = \begin{pmatrix} \boldsymbol{A} & \boldsymbol{B} \\ \boldsymbol{B}^T & \boldsymbol{D} \end{pmatrix} \begin{Bmatrix} \bar{\boldsymbol{e}} \\ \bar{\boldsymbol{\kappa}} \end{Bmatrix} \tag{4}$$

where $\boldsymbol{F}$ and $\boldsymbol{M}$ are the cross-sectional force and moment stress vectors in the deformed beam basis, and $\bar{\boldsymbol{e}}$ and $\bar{\boldsymbol{\kappa}}$ vectors are defined as follows: $\bar{\boldsymbol{e}} = \{\bar{e}_{11} \;\; 2\bar{e}_{12} \;\; 2\bar{e}_{13}\}^T$, $\bar{\boldsymbol{\kappa}} = \{\kappa_1 \;\; \kappa_2 \;\; \kappa_3\}^T$. The matrices $\boldsymbol{A}$, $\boldsymbol{B}$, and $\boldsymbol{D}$ are 3×3 matrices that depend on the material properties and the geometry of the cross section.

Aerodynamics

The two-dimensional, quasi-steady lift theory based on Greenberg's extension[37] of Theodorsen's theory for a two-dimensional airfoil undergoing unsteady motion in an incompressible flow is considered in the present work. The components of resultant velocity $\boldsymbol{U}$ in the deformed blade coordinate system are given by

$$\begin{Bmatrix} U_R \\ U_T \\ U_P \end{Bmatrix} = \boldsymbol{T} \begin{Bmatrix} \dot{u}_1 - \Omega R_{02} - \Omega R\mu \cos\psi \\ \dot{u}_2 + \Omega R_{01} - \Omega R\mu \sin\psi \\ \dot{u}_3 + \Omega R\lambda_i \end{Bmatrix} \tag{5}$$

where $\dot{u}_i$ is the component of elastic velocity vector $\dot{\boldsymbol{u}}$ of blade and R_{0i} is the component of position vector $\boldsymbol{R}$ of an arbitrary point of the cross section in the deformed blade configuration. The advance ratio μ and the inflow ratio λ_i are defined as nondimensionalized forward speed $V/\Omega R$ and induced velocity $v_{\mathrm{id}}/\Omega R$, respectively. The Drees linear inflow model is used for the rotor inflow distribution. The effects of compressibility and reversed flow are also included in the aerodynamic models. The compressibility effect is applied using the Prandtl–Glauert theory, and the reverse flow effect is applied considering tangential component of resultant velocity $\boldsymbol{U}$.

Blade Steady Response and Coupled Trim Analysis

The nonlinear, periodic steady response is obtained using a time finite element technique.[36] The virtual energy expression for the Hamilton's weak form can be obtained as follows:

$$\int_{\psi_i}^{\psi_f} \delta \boldsymbol{y}^T \boldsymbol{l}\, \mathrm{d}\psi = \delta \boldsymbol{y}^T \boldsymbol{b}\Big|_{\psi_i}^{\psi_f} \tag{6}$$

where

$$\delta \boldsymbol{y} = \begin{Bmatrix} \delta \boldsymbol{q} \\ \delta \dot{\boldsymbol{q}} \end{Bmatrix}, \qquad \boldsymbol{l} = \begin{Bmatrix} \boldsymbol{L}_{\dot{q}} \\ \boldsymbol{L}_q + \boldsymbol{Q} \end{Bmatrix}, \qquad \boldsymbol{b} = \begin{Bmatrix} \boldsymbol{0} \\ \boldsymbol{p} \end{Bmatrix} \tag{7}$$

where $\boldsymbol{Q}$ is the generalized force and $\boldsymbol{L}$ is the Lagrangian of the system. $\boldsymbol{L}_{\dot{q}}$ and $\boldsymbol{L}_q$ are the partial derivatives of $\boldsymbol{L}$ with respect to generalized coordinates $\dot{\boldsymbol{q}}$ and $\boldsymbol{q}$, respectively, which are composed of displacements and Euler angles, whereas $\boldsymbol{p} = \boldsymbol{L}_{\dot{q}}$ is the column vector of the generalized moment. ψ_i and ψ_f represent the initial and final states of nondimensionalized time, respectively. Using a first-order Taylor-series expansion of the left-hand side of Eq. (6) with respect to a given state vector $\bar{\boldsymbol{y}}$, the following governing equation can be derived in an incremental form:

$$\int_{\psi_i}^{\psi_f} \delta \boldsymbol{y}^T \bar{\boldsymbol{l}}\, \mathrm{d}\psi + \int_{\psi_i}^{\psi_f} \delta \boldsymbol{y}^T \bar{\boldsymbol{K}} \Delta \boldsymbol{y}\, \mathrm{d}\psi = \delta \boldsymbol{y}^T \boldsymbol{b}\Big|_{\psi_i}^{\psi_f} \tag{8}$$

where the local tangent matrix $\bar{\boldsymbol{K}}$ is defined as

$$\bar{\boldsymbol{K}} = \begin{pmatrix} \boldsymbol{L}_{\dot{q}\dot{q}} & \boldsymbol{L}_{\dot{q}q} \\ \boldsymbol{L}_{q\dot{q}} + \boldsymbol{Q}_{\dot{q}} & \boldsymbol{L}_{qq} + \boldsymbol{Q}_q \end{pmatrix} \tag{9}$$

where $\boldsymbol{L}_{\dot{q}\dot{q}}$, $\boldsymbol{L}_{\dot{q}q}$, $\boldsymbol{L}_{qq}$, $\boldsymbol{Q}_{\dot{q}}$, and $\boldsymbol{Q}_q$ indicate the second and first derivatives with respect to the subscripts, respectively. The time period for one revolution is discretized into a number of time elements with cubic variation, and after assembling elements in a global system a periodic boundary condition is imposed by folding the row and column of the assembled matrix and vector.

The propulsive vehicle trim analysis is fully coupled with earlier blade steady response analysis to solve the blade response, pilot control inputs, and vehicle orientation simultaneously. The vehicle trim solution is calculated from the overall nonlinear vehicle equilibrium equations: three force equations (vertical, longitudinal, and lateral) and three moment equations (pitch, roll, and yaw). Fixed-frame hub loads are also calculated by summing the contributions from individual blades.

Aeroelastic Stability

For stability analysis the blade perturbation equations of motion are linearized about the equilibrium position:

$$\begin{Bmatrix} \ddot{\tilde{\boldsymbol{q}}} \\ \tilde{\boldsymbol{q}} \end{Bmatrix} = \begin{pmatrix} \boldsymbol{L}_{\dot{q}\dot{q}}(\boldsymbol{q}_0) & \boldsymbol{L}_{\dot{q}q}(\boldsymbol{q}_0) \\ \boldsymbol{L}_{q\dot{q}}(\boldsymbol{q}_0) + \boldsymbol{Q}_{\dot{q}}(\boldsymbol{q}_0) & \boldsymbol{L}_{qq}(\boldsymbol{q}_0) + \boldsymbol{Q}_q(\boldsymbol{q}_0) \end{pmatrix} \begin{Bmatrix} \dot{\tilde{\boldsymbol{q}}} \\ \tilde{\boldsymbol{q}} \end{Bmatrix} \tag{10}$$

where $\boldsymbol{q}_0$ is the nonlinear trim solution as a function of azimuth angle and $\tilde{\boldsymbol{q}}(t)$ is small perturbation about the periodic equilibrium position $\boldsymbol{q}_0$. These equations contain periodic coefficients and can be integrated numerically in time for the proper initial conditions of displacements and velocities. The initial value of the perturbed blade motion is taken to be 10% of the equilibrium position at a proper time position. From the initial perturbation the blade is set free to move, and the blade perturbation equations of motion are integrated by the fourth-order Runge–Kutta method. To obtain more accurate modal damping and frequency, the initial perturbation of the blade is given only in the particular mode of interest. Once the time histories of the blade lag, flap, and torsional deflections are known, the modal damping and frequency of any desired mode can be determined from the moving block analysis.[38]

Numerical Results and Discussion

Aeroelastic response and stability analyses of isotropic and composite rotor blades are performed using the large deflection-type beam theory. Nonlinear periodic steady response is obtained by integrating the full finite element equations in time, and aeroelastic stability is obtained from time histories of perturbed deflections under small perturbations assumption about the nonlinear periodic equilibrium position. In the present investigation the modal analysis using linear rotating vibration modal bases is confirmed to be improper because of poor results in the nonlinear steady response analysis. Therefore, the present results obtained by the full finite element analysis using the large deflection-type beam theory are compared with the previous published results obtained by the modal analysis using the moderate deflection-type beam theory. The accuracy of various modal bases in the nonlinear modal analysis of helicopter rotor blades is investigated by comparing with results obtained by the full finite element analysis in Ref. 39. Bauchau and Guernsey[39] mentioned that the full finite element analysis is preferable in the aeroelastic analysis with coupling of aerodynamics and structural dynamics of helicopter rotor blades. The present paper focuses on investigating nonlinear kinematic effects caused by large deflections by comparing two models.

Isotropic Rotor Blade

The blade is discretized into five four-noded cubic elements in space domain, and the time period of one rotor revolution is discretized into seven four-noded cubic elements in time domain for reasonably good convergence. The convergence test of the present beam model has been performed for the nonlinear static analysis of composite beam is Ref. 20. The structural properties and vehicle configuration of the isotropic rotor blade used for numerical computation are present in Table 1, and the first flap, lag, and torsional frequencies of this soft-inplane hingeless rotor are 1.13, 0.70, and 4.47/rev, respectively. Figure 2 shows flap and lag tip deflections of the blade for one revolution at an advance ratio $\mu = 0.1$. The present analysis is compared with the previous results given in Ref. 40, and a good correlation between these two results is shown in the Fig. 2. The results of Ref. 40 are obtained using the modal analysis with a modal basis of eight coupled rotating natural modes (2 flap, 2 lag, 2 torsion, and 2 axial modes) based on the moderate deflection-type beam theory, and the present results are obtained using the full finite element analysis based on the large deflection-type beam theory. As shown in Figs. 3 and 4, the agreement between two results is quite good for advance ratios $\mu = 0.2$ and 0.3, but some

Table 1 Vehicle and structural properties of isotropic rotor blade

Parameter	Value
Main rotor	
Number of blades	4
Blade aspect ratio c/R	0.055
Solidity σ	0.07
Thrust level C_W/σ	0.07
Lock number	5.5
c_l	$2\pi\alpha$
c_d	0.01
$EI_y/m_0\Omega^2R^4$	0.01080
$EI_z/m_0\Omega^2R^4$	0.02680
$GJ/m_0\Omega^2R^4$	0.00615
k_A/R	0.0290
k_{m1}/R	0.0132
k_{m2}/R	0.0247
Vehicle	
Longitude and latitude offsets, $x_{c.g.}/R$, $y_{c.g.}/R$	0.0, 0.0
c.g. below hub, h/R	0.2
Flat plate area $f/\pi R^2$	0.01

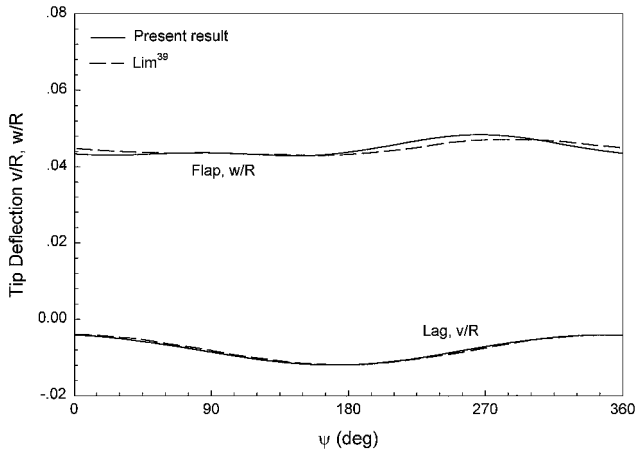

Fig. 2 Steady tip deflections of isotropic blade in forward flight ($\theta = 0.1$ and $C_T/\sigma = 0.07$).

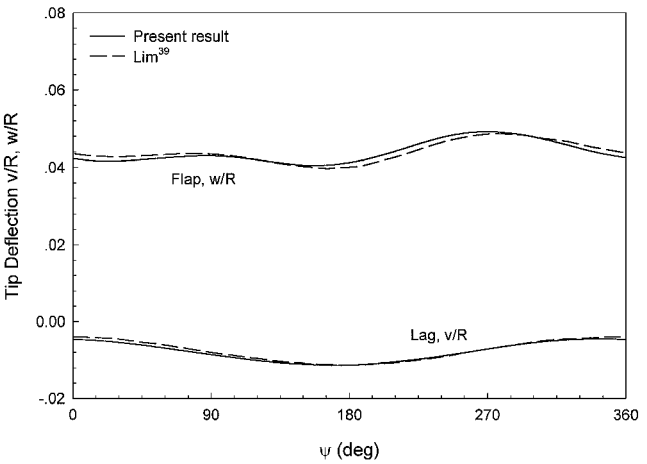

Fig. 3 Steady tip deflections of isotropic blade in forward flight ($\theta = 0.2$ and $C_T/\sigma = 0.07$).

differences appear as the forward speed increases. Figure 5 shows the time histories for blade motions obtained from an initial perturbation about the known periodic equilibrium deflections under small perturbations assumption. To obtain the time histories of individual modes, the initial perturbation of the blade is given only in the particular mode of interest. However, there are some high-frequency components in the perturbed lag tip deflections because the initial value is taken to be static deflection of individual modes.

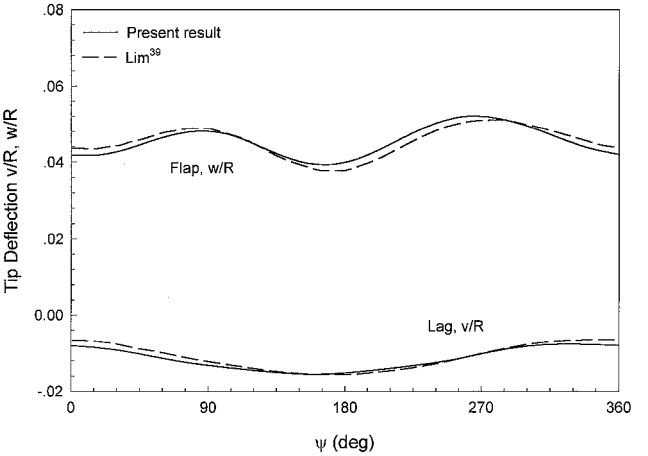

Fig. 4 Steady tip deflections of isotropic blade in forward flight ($\theta = 0.3$ and $C_T/\sigma = 0.07$).

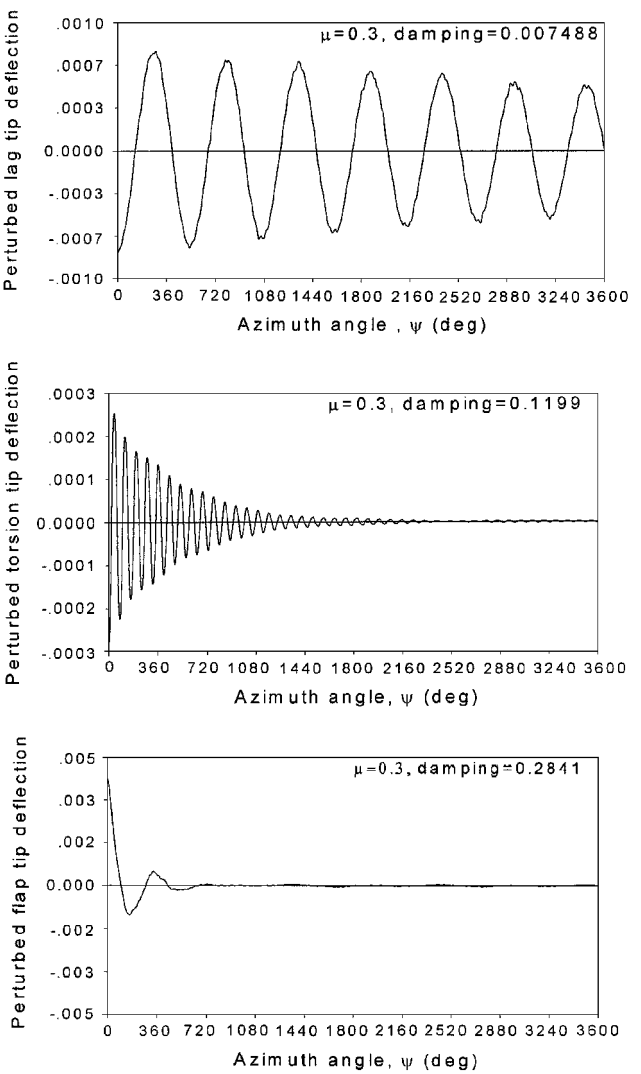

Fig. 5 Time histories of perturbed motions from initial perturbations ($\theta = 0.3$ and $C_T/\sigma = 0.07$).

The results show that the lag mode damping is the smallest one, and the flap mode damping is the biggest one. The lag mode stability is generally treated as an important factor of aeroelastic stability analysis of hingeless rotor blades because the aerodynamic damping of the lag mode is the mildest one. Lag, flap, and torsion mode stability results for different advance ratios are illustrated in Figs. 6 and 7. The modal damping characteristics of the present results are determined through the moving block analysis for the time histories.

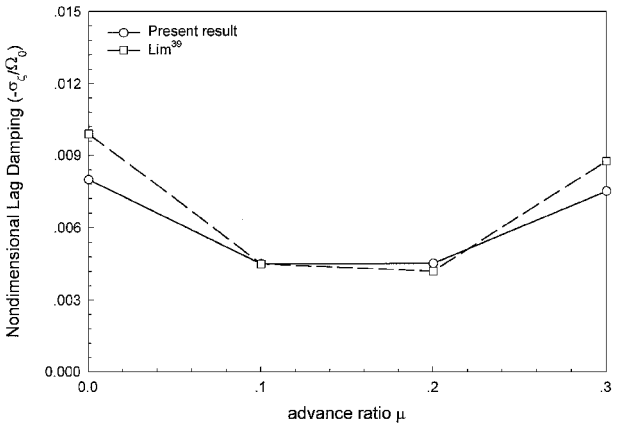

Fig. 6 First lag mode damping of isotropic blade with different advance ratio ($C_T/\sigma = 0.07$).

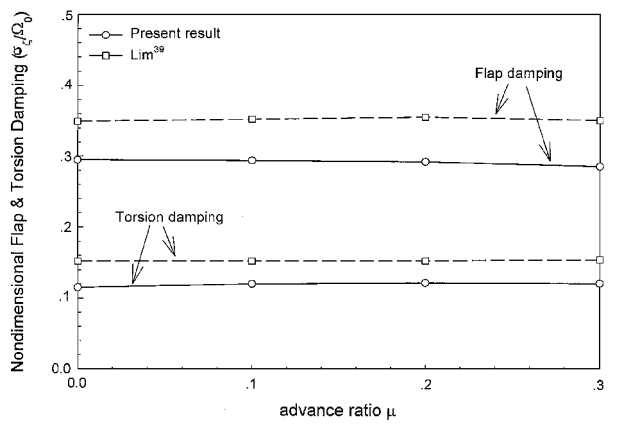

Fig. 7 First flap and torsion mode damping of isotropic blade with different advance ratio ($C_T/\sigma = 0.07$).

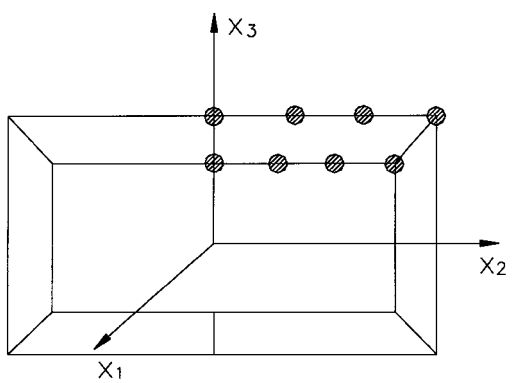

Fig. 8 Cross-sectional modeling of composite box beam.

The observation is made that the damping obtained from the present analysis generally has a lower value than that of Ref. 40 from the Floquet theory with a modal basis. The modal basis used for the stability calculation in Ref. 40 contains six coupled rotating natural modes except axial modes (2 flap, 2 lag, and 2 torsion) obtained about the mean deflected position. Discrepancies of the steady response results and the different methods of the stability analysis give the differences between the two results.

Composite Rotor Blade

The sectional elastic constants including the effects of general warping in and out of plane are obtained in unloaded condition using the refined cross-sectional finite element method. Then, these sectional elastic constants are used for the one-dimensional global analysis. Six cross-sectional elements are used for the computation of sectional elastic constants depicted in Fig. 8. The one-dimensional global analysis is performed using five four-noded cubic elements for reasonably good convergence. The static and dynamic analyses and aeroelastic stability analysis in hover condition of composite box beams based on the large deflection-type beam theory have been validated in Refs. 20 and 35.

Table 2 Rotating natural frequencies of symmetric layup box beam[a]

	Frequency, Hz			
Mode	Experiment	Detailed finite element method	Smith and Chopra[29]	Present
Flap 1	28.60	27.33	28.13	27.12
Flap 2	135.0	133.6	139.8	131.9
Lag 1	39.50	38.66	42.85	38.39
Lag 2	NA	236.3	261.3	236.9
Torsion 1	NA	872.9	936.1	935.9

[a]Top and bottom: $(30)_6$; right and left: $(30/-30)_3$ at $\Omega = 1014$ rpm.

The material properties for the present analysis are chosen as AS4/3501-6 graphite/epoxy with the following properties: $E_{11} = 20.59$ msi (141.9 Gpa), $E_{22} = E_{33} = 1.42$ msi (9.8 Gpa), $G_{12} = G_{13} = 0.89$ msi (6.14 Gpa), $G_{23} = 0.47$ msi (3.24 Gpa), $\nu_{12} = \nu_{13} = 0.42$, $\nu_{23} = 0.5$, and mass density is 0.0001352 lb-s^2/in.^{4} (1445 kg/m^3). The beam length is 33.25 in. (0.845 m), the width 0.953 in. (0.024 m), the depth 0.537 in. (0.014 m), and the ply thickness 0.005 in. (0.127 mm). The composite box beam with the $[30]_6$ symmetric layup[9] under the rotation of 1014 rpm is used for the calculation of rotating natural frequencies. For comparison five natural modes are examined, and the present results are shown in Table 2. The experimental data are taken from Ref. 9. Detailed finite element results are obtained using the analysis developed by Stemple and Lee.[13] Because the treatment of the cross-section warping is coupled with the treatment of the beam bending, torsion, and extension, Stemple and Lee's approach has more degrees of freedom than the present approach. Numerical results from Smith and Chopra's analysis[29] are also compared. The agreement between the results of three models and the experimental data for the natural frequencies is good, but the present result is closer to the detailed finite element results than that of Ref. 29. This may be caused by the more accurate modeling of the cross section in the composite box beam. Table 3 shows rotating natural frequencies of two layup configurations that are used for the aeroelastic response and stability analyses. In these layup configurations the width of the outer box spar is 4.2 in. (0.107 m), the depth of the outer spar is 2.2 in. (0.056 m), and each of the four spar walls contains 26 graphite/epoxy plies. Although there are some differences caused by the cross-sectional analysis, the correlation of the two results is quite good.

Aeroelastic analysis of the preceding two layup configurations is performed to investigate the effects of large deflection. Eight four-noded cubic elements are used to model the period of one rotor revolution. The properties of the vehicle and rotor are given in Table 4. The present results based on the large deflection-type beam theory are compared with Smith and Chopra's results[29] based on the moderate deflection-type beam theory. The present analysis used the full finite element method in the displacement-based formulation, and Ref. 29 used the modal method with the modal basis of eight normal modes (3 bending torsion, 2 bending, 2 torsion bending, and 1 axial). Figures 9 and 10 show the flap and lag tip deflections of the baseline case (Table 3) for advance ratio $\mu = 0.2$ and 0.35, respectively. The baseline case exhibits no elastic coupling. The present results are compared with those of Ref. 29. There are some differences between the results of two models, and these differences increase as the forward speed increases. Because the amplitudes of the nondimensional tip deflections are larger than those of the isotropic blade case, nonlinear kinematic effects exist on a large scale, and the differences become larger in the composite blade case. Because differences of frequencies between two models are very small, the effects of these differences may be negligible in the analysis. However, because the nonlinear kinematic effects are large, it is considered that the effects of the large deflection and the assumption of the modal analysis are not negligible. Discrepancies between the modal analysis and the full finite element analysis are investigated for four numerical examples of helicopter rotor blades

Table 3 Rotating natural frequencies of composite box beams at $\Omega = 383$ rpm

Configuration	Mode	Frequency, /rev	
		Smith and Chopra[29]	Present
Baseline	Flap 1	1.146	1.144
Top $[0_3/(15/-15)_3/(45/-45)_2]_s$	Flap 2	3.389	3.379
Bottom $[0_3/(15/-15)_3/(45/-45)_2]_s$	Flap 3	7.416	7.351
Right $[0_3/(15/-15)_3/(45/-45)_2]_s$	Lag 1	0.747	0.746
Left $[0_3/(15/-15)_3/(45/-45)_2]_s$	Lag 2	4.315	4.304
	Torsion 1	4.590	4.622
	Torsion 2	13.60	13.62
Symmetric B	Flap 1	1.142	1.139
Top $[0_3/(15)_6/(45/-45)_2]_s$	Flap 2	3.346	3.322
Bottom $[0_3/(15)_6/(45/-45)_2]_s$	Flap 3	7.265	7.151
Right $[0_3/(15/-15)_3/(45/-45)_2]_s$	Lag 1	0.747	0.737
Left $[0_3/(15/-15)_3/(45/-45)_2]_s$	Lag 2	4.314	4.250
	Torsion 1	4.590	4.617
	Torsion 2	13.62	13.68

Table 4 Vehicle and structural properties of composite rotor blade

Parameter	Value
Main rotor	
Number of blades	4
Radius, ft (m)	16.2 (4.94)
Hover tip speed, ft/s (m/s)	650 (198)
Blade aspect ratio, c/R	0.08
Solidity, σ	0.1
Thrust level, C_W/σ	0.07
Lock number	6.34
c_l	5.73α
c_d	$0.0095 + 0.2\alpha^2$
Mass per unit length, slug/ft (kg/m)	0.135 (47.9)
k_{m1}^2/R, k_{m2}^2/R	0.0001, 0.0004
Hub lenth, x_{hub}/R	0.04
Aerodynamic root cutout, x_{root}/R	0.10
Tail rotor and horizontal tail	
Tail rotor radius, ft (m)	3.24 (0.988)
Tail rotor solidity, σ_{tr}	0.15
Tail rotor gear ratio, $\Omega_{\text{tr}}/\Omega_{\text{mr}}$	5.0
Tail rotor location, x_{tr}/R	1.2
Tail rotor above c.g., h_{tr}/R	0.2
$(c_l)_{\text{tr}}$	6.0α
Horizontal tail location, x_{ht}/R	0.95
Horizontal tail planform area, $S_{\text{ht}}/\pi R^2$	0.011
$(c_l)_{\text{ht}}$	6.0α
Vehicle	
Total vehicle weight, lb (N)	5800 (25,800)
Longitude and latitude offsets, $x_{\text{c.g.}}/R$, $y_{\text{c.g.}}/R$	0.0, 0.0
c.g. below hub, h/R	0.2
Flat plate area, $f/\pi R^2$	0.01

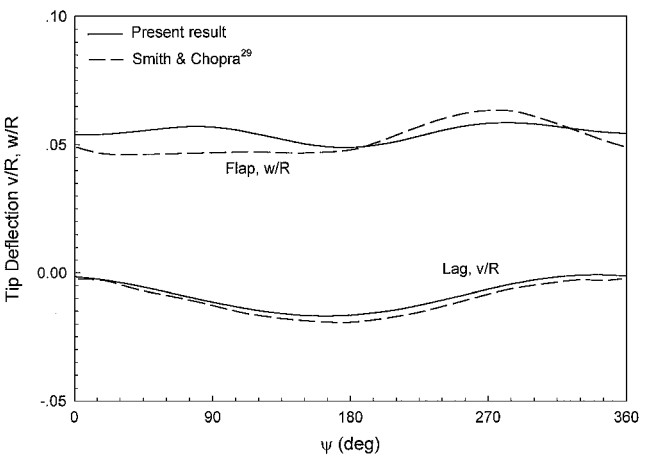

Fig. 9 Steady tip deflections of composite blade for baseline case in forward flight ($\theta = 0.2$ and $C_T/\sigma = 0.07$).

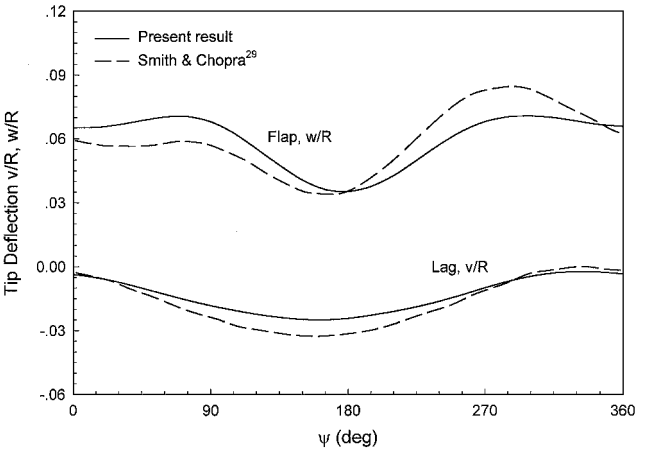

Fig. 10 Steady tip deflections of composite blade for baseline case in forward flight ($\theta = 0.35$ and $C_T/\sigma = 0.07$).

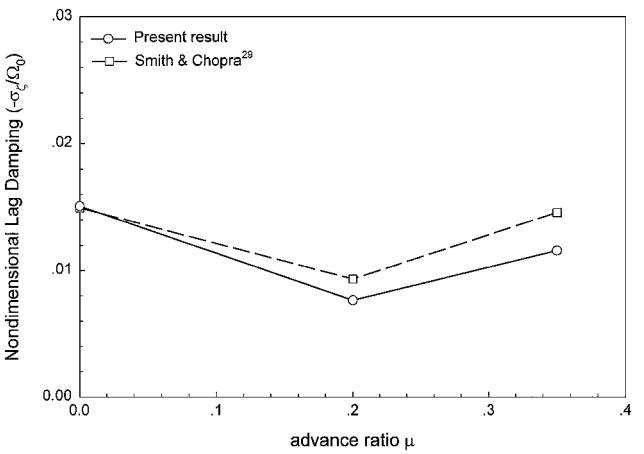

Fig. 11 First lag mode damping of composite blade for baseline case with different advance ratio ($C_T/\sigma = 0.07$).

in Ref. 39. Figure 11 shows the variation of lag mode damping with advance ratio $\mu = 0$, 0.2, and 0.35. The present results are obtained using the moving block analysis from time histories of perturbed deflections, and Smith and Chopra's results are obtained using the Floquet theory with the modal basis. The results of two models are very close in hover condition, but the differences appear as the forward speed increases. An aspect of the tip deflections of the symmetric B case (Table 3) is similar to that of baseline case, and the variation of lag mode damping of the symmetric B case is present in Fig. 12. Symmetric B case exhibits pitch-flap and extension-lag shear couplings, and this case has lower values of lag mode damping than the baseline case. It shows some differences between the results of two models in hover condition, and the differences increase as

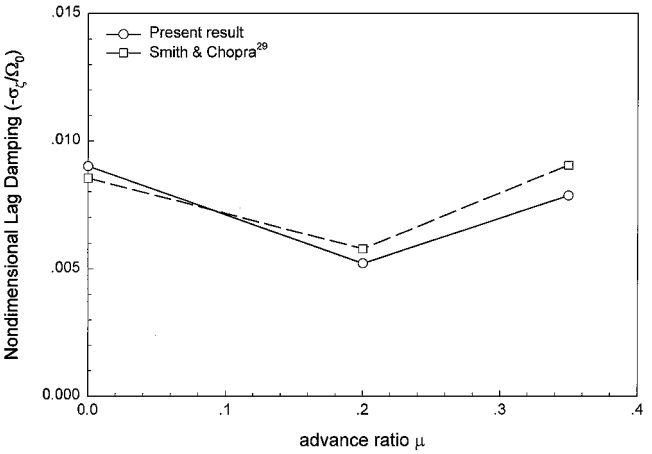

Fig. 12 First lag mode damping of composite blade for symmetric B case with different advance ratio ($C_T/\sigma = 0.07$).

the forward speed increases. The full finite element analysis using the large deflection-type beam theory gives lower values in the lag mode damping, and it may be because of the different methods of approach. When the deflection is large, the full finite element analysis should be used instead of the modal approach to predict the aeroelastic response and stability characteristics.

Conclusions

In this paper the aeroelastic analysis of hingeless rotor blades in forward flight has been performed. The finite element formulation is obtained using the large deflection-type model, which is not based on an ordering scheme and includes all kinematic nonlinear effects. Nonlinear, periodic blade steady response is computed using the time finite element method on the full finite element equation with full coupling of the propulsive vehicle trim. Stability characteristics are determined through the moving block analysis for the time histories. The periodic steady tip deflections and the aeroelastic modal damping for isotropic and composite rotor blades are compared with those obtained by the modal approach using the moderate deflection-type beam theory. The results show that the effects of the large deflection and the assumption of the modal analysis somewhat affect the steady equilibrium and rotor stability. Although the cross-sectional analysis is different, the results of steady response and stability analyses are mainly influenced on the nonlinear kinematic effects. The nonlinear kinematic effects greatly affect the steady response as the forward speed increases. The aeroelastic modal damping is predicted smaller than that of the modal analysis using the moderate deflection-type beam theory. The conclusion is made that the full finite element methods using the large deflection-type beam theory should be preferred for the accurate prediction of the hingeless rotor behavior with large deflection.

References

[1]Friedmann, P. P., "Rotary-Wing Aeroelasticity with Application to VTOL Vehicles," *Proceedings of the AIAA/ASME/ASCE/AHS/ACS 31th Structures, Structural Dynamics, and Materials Conference*, AIAA, Washington, DC, 1990, pp. 1624–1670.

[2]Hodges, D. H., "Review of Composite Rotor Blade Modeling," *AIAA Journal*, Vol. 28, No. 3, 1990, pp. 561–565.

[3]Rehfield, L. W., Atilgan, A. R., and Hodges, D. H., "Nonclassical Behavior of Thin-Walled Composite Beams with Closed Cross Sections," *Journal of the American Helicopter Society*, Vol. 35, No. 2, 1990, pp. 42–50.

[4]Hodges, D. H., and Dowell, E. H., "Nonlinear Equations of Motion for Elastic Bending and Torsion of Twisted Non-Uniform Rotor Blades," NASA TN D-7818, Dec. 1974.

[5]Chandra, R., Stemple, A. D., and Chopra, I., "Thin-Walled Composite Beams Under Bending, Torsional, and Extensional Loads," *Journal of Aircraft*, Vol. 27, No. 7, 1990, pp. 619–626.

[6]Smith, E. C., and Chopra, I., "Formulation and Evaluation of Analytical Model for Composite Box-Beams," *Journal of the American Helicopter Society*, Vol. 36, No. 3, 1991, pp. 23–35.

[7]Chandra, R., and Chopra, I., "Experimental and Theoretical Analysis of Composite I-Beams with Elastic Couplings," *AIAA Journal*, Vol. 29, No. 12, 1991, pp. 2197–2205.

[8]Kosmatka, J. B., and Friedmann, P. P., "Vibration Analysis of Composite Turbopropellers Using a Nonlinear Beam-Type Finite Element Approach," *AIAA Journal*, Vol. 27, No. 11, 1989, pp. 1606–1614.

[9]Chandra, R., and Chopra, I., "Experimental and Theoretical Investigation of the Vibration Characteristics of Rotating Composite Box Beams," *Journal of Aircraft*, Vol. 29, No. 4, 1992, pp. 657–664.

[10]Epps, J. J., and Chandra, R., "The Natural Frequencies of Rotating Composite Beams with Tip Sweep," *Journal of the American Helicopter Society*, Vol. 41, No. 1, 1996, pp. 29–36.

[11]Bauchau, O. A., and Hong, C. H., "Large Displacement Analysis of Naturally Curved and Twisted Composite Beams," *AIAA Journal*, Vol. 25, No. 11, 1987, pp. 1469–1475.

[12]Bauchau, O. A., and Hong, C. H., "Nonlinear Composite Beam Theory," *Journal of Applied Mechanics*, Vol. 55, No. 1, 1988, pp. 156–163.

[13]Stemple, A. D., and Lee, S. W., "Large Deflection Static and Dynamic Finite Element Analysis of Composite Beams with Arbitrary Cross Sectional Warping," *Proceedings of the AIAA/ASME/ASCE/AHS/ACS 30th Structures, Structural Dynamics, and Materials Conference*, AIAA, Washington, DC, 1989, pp. 1788–1798.

[14]Minguet, P., and Dugundji, J., "Experiments and Analysis for Composite Blades Under Large Deflections Part I: Static Behavior," *AIAA Journal*, Vol. 28, No. 9, 1990, pp. 1573–1579.

[15]Hodges, D. H., "A Mixed Variational Formulation Based on Exact Intrinsic Equations for Dynamics of Moving Beams," *International Journal of Solids and Structures*, Vol. 26, No. 11, 1990, pp. 1253–1273.

[16]Atilgan, A. R., and Hodges, D. H., "Unified Nonlinear Analysis for Nonhomogeneous Anisotropic Beams with Closed Cross Sections," *AIAA Journal*, Vol. 29, No. 11, 1991, pp. 1990–1999.

[17]Hodges, D. H., Shang, X., and Cesnik, C. E. S., "Finite Element Solution of Nonlinear Intrinsic Equations for Curved Composite Beams," *Journal of the American Helicopter Society*, Vol. 41, No. 4, 1996, pp. 313–321.

[18]Minguet, P., and Dugundji, J., "Experiments and Analysis for Composite Blades Under Large Deflections Part 2: Dynamic Behavior," *AIAA Journal*, Vol. 28, No. 9, 1990, pp. 1579–1588.

[19]Hodges, D. H., Atilgan, A. R., Fulton, M. V., and Rehfield, L. W., "Free-Vibration Analysis of Composite Beams," *Journal of the American Helicopter Society*, Vol. 36, No. 3, 1991, pp. 36–47.

[20]Jeon, S. M., Cho, M. H., and Lee, I., "Static and Dynamic Analysis of Composite Box Beams Using Large Deflection Theory," *Computers and Structures*, Vol. 57, No. 4, 1995, pp. 635–642.

[21]Libove, C., "Stresses and Rate of Twist in Single-Cell Thin-Walled Beams with Anisotropic Walls," *AIAA Journal*, Vol. 26, No. 10, 1988, pp. 1006–1118.

[22]Giavotto, V., Borri, M., Mantegazza, P., and Ghiringhelli, G., "Anisotropic Beam Theory and Applications," *Computers and Structures*, Vol. 16, Nos. 1–4, 1983, pp. 403–413.

[23]Borri, M., Ghiringhelli, G. L., and Merlini, T., "Linear Analysis of Naturally Curved and Twisted Anisotropic Beams," *Composites Engineering*, Vol. 2, Nos. 5–7, 1992, pp. 433–456.

[24]Cesnik, C. E. S., and Hodges, D. H., "VABS: A New Concept for Composite Rotor Blade Cross-Sectional Modeling," *Journal of the American Helicopter Society*, Vol. 42, No. 1, 1997, pp. 27–38.

[25]Hong, C. H., and Chopra, I., "Aeroelastic Stability Analysis of a Composite Rotor Blade," *Journal of the American Helicopter Society*, Vol. 30, No. 2, 1985, pp. 57–67.

[26]Yamane, T., and Friedmann, P. P., "Aeroelastic Tailoring Analysis for Preliminary Design of Advanced Turbo Propellers with Composite Blades," *Journal of Aircraft*, Vol. 30, No. 1, 1993, pp. 119–126.

[27]Panda, B., and Chopra, I., "Dynamics of Composite Rotor Blades in Forward Flight," *Vertica*, Vol. 11, No. 1/2, 1987, pp. 187–209.

[28]Rand, O., "Periodic Response of Thin-Walled Composite Helicopter Rotor Blades," *Journal of the American Helicopter Society*, Vol. 36, No. 4, 1991, pp. 3–11.

[29]Smith, E. C., and Chopra, I., "Aeroelastic Response and Blade Loads of a Composite Rotor in Forward Flight," *Proceedings of the AIAA/ASME/ASCE/AHS/ACS 33rd Structures, Structural Dynamics, and Materials Conference*, AIAA, Washington, DC, 1992, pp. 1996–2014.

[30]Cho, M. H., and Lee, I., "Aeroelastic Stability of Hingeless Rotor Blade in Hover Using Large Deflection Theory," *AIAA Journal*, Vol. 32, No. 7, 1994, pp. 1472–1477.

[31]Cho, M. H., and Lee, I., "Aeroelatic Analysis of Multibladed Hingeless Rotors in Hover," *AIAA Journal*, Vol. 33, No. 12, 1995, pp. 2348–2353.

[32]Cho, M. H., Jeon, S. M., Woo, S. H., and Lee, I., "Refined Aeroelastic Analysis of Hingeless Rotor Blades in Hover," *Journal of Aircraft*, Vol. 34, No. 3, 1997, pp. 408–415.

[33]Fulton, M. V., and Hodges, D. H., "Aeroelastic Stability of Composite Hingeless Rotor Blades in Hover—Part I: Theory," *Mathematical and Computer Modeling*, Vol. 18, No. 3/4, 1993, pp. 1–17.

[34]Fulton, M. V., and Hodges, D. H., "Aeroelastic Stability of Composite Hingeless Rotor Blades in Hover—Part II: Results," *Mathematical and Computer Modeling*, Vol. 18, No. 3/4, 1993, pp. 19–35.

[35]Jeon, S. M., Cho, M. H., and Lee, I., "Aeroelastic Analysis of Composite Rotor Blades in Hover," *Computers and Structures*, Vol. 66, No. 1, 1998, pp. 59–67.

[36]Borri, M., "Helicopter Rotor Dynamics by Finite Element Time Approximations," *Computers and Mathematics with Applications*, Vol. 12A, No. 1, 1986, pp. 149–160.

[37]Greenberg, J. M., "Airfoil in Sinusoidal Motion in a Pulsating Stream," NACA TN-1326, June 1947.

[38]Hammond, C. E., and Doggett, R. V., Jr., "Determination of Subcritical Damping by Moving-Block/Randomdec Application," NASA Symposium on Flutter Testing Techniques, Oct. 1975.

[39]Bauchau, O. A., and Guernsey, D., "On the Choice of Appropriate Bases for Nonlinear Dynamic Modal Analysis," *Journal of the American Helicopter Society*, Vol. 38, No. 4, 1993, pp. 28–36.

[40]Lim, J. W., "Aeroelastic Optimization of a Helicopter Rotor," Ph.D. Dissertation, Dept. of Aerospace Engineering, Univ. of Maryland, College Park, MD, April 1988.

A. N. Palazotto
Associate Editor